ORIGINAL ARTICLE

Cancer Science WILEY

Programmed death (PD)-1/PD-ligand 1 blockade mediates antiangiogenic effects by tumor-derived CXCL10/11 as a potential predictive biomarker

Atsushi Mitsuhashi[1] | Kensuke Kondoh[1] | Kazuki Horikawa[2] | Kazuya Koyama[1] | Na Thi Nguyen[1] | Tania Afroj[1] | Hiroto Yoneda[1] | Kenji Otsuka[1] | Hirokazu Ogino[1] | Hiroshi Nokihara[1] | Tsutomu Shinohara[3] | Yasuhiko Nishioka[1,4] ⓘD

[1]Department of Respiratory Medicine and Rheumatology, Graduate School of Biomedical Sciences, Tokushima University, Tokushima, Japan

[2]Department of Optical Imaging, Graduate School of Biomedical Sciences, Tokushima University, Tokushima, Japan

[3]Department of Community Medicine for Respirology, Graduate School of Biomedical Sciences, Tokushima University, Tokushima, Japan

[4]Department of Community Medicine for Rheumatology, Graduate School of Biomedical Sciences, Tokushima University, Tokushima, Japan

Correspondence
Yasuhiko Nishioka, 3-18-15 Kuramoto-cho, Tokushima, Tokushima 770-8503, Japan.
Email: yasuhiko@tokushima-u.ac.jp

Funding information
Japan Society for the Promotion of Science (JSPS) KAKENHI , Grant/Award Number: 16H05309 (to YN), 19K16746 (to AM); grant to the Diffuse Lung Diseases Research Group from the Ministry of Health, Labour and Welfare, Japan (to YN)

Abstract

Immune checkpoint inhibitor (ICI) programmed death (PD)-1/PD-ligand 1 (PD-L1) blockade has been approved for various cancers. However, the underlying antitumor mechanisms mediated by ICIs and the predictive biomarkers remain unclear. We report the effects of anti-PD-L1/PD-1 Ab in tumor angiogenesis. In syngeneic mouse models, anti-PD-L1 Ab inhibited tumor angiogenesis and induces net-like hypoxia only in ICI-sensitive cell lines. In tumor tissue and serum of ICI-sensitive cell line-bearing mice, interferon-γ (IFN-γ) inducible angiostatic chemokines CXCL10/11 were upregulated by PD-L1 blockade. In vitro, *CXCL10/11* gene upregulation by IFN-γ stimulation in tumor cell lines correlated with the sensitivity of PD-L1 blockade. The CXCL10/11 receptor CXCR3-neutralizing Ab or CXCL11 silencing in tumor cells inhibited the antiangiogenic effect of PD-L1 blockade in vivo. In pretreatment serum of lung carcinoma patients receiving anti-PD-1 Ab, the concentration of CXCL10/11 significantly correlated with the clinical outcome. Our results indicate the antiangiogenic function of PD-1/PD-L1 blockade and identify tumor-derived CXCL10/11 as a potential circulating biomarker of therapeutic sensitivity.

KEYWORDS
angiogenesis, biomarker, CXCL10/11, immune checkpoint inhibitor, lung cancer

1 | INTRODUCTION

Immune checkpoint inhibitors (ICIs) targeting programmed death 1 (PD-1) and its ligand, PD-L1, have established clinical benefit in various types of malignancies.[1-4] The PD-1/PD-L1 axis is known to influence tumor microenvironment, including T cells, macrophages, dendritic cells, and tumor cells. It is well established that the reinvigoration of pre-existing T cells and/or induction of novel clones of CTLs play central roles in the antitumor effects mediated by PD-1/PD-L1 blockade.[5-8] However, as macrophages aside from

T cells are also directly involved in antitumor effects through the phagocytic function,[9] the major mechanisms underlying antitumor effects mediated by PD-1/PD-L1 blockade remain incompletely understood.

Recent reports have revealed that ICIs have stronger effects on some specific populations of tumor patients than on others. For example, in non-small-cell lung carcinoma (NSCLC) patients, some predictive biomarkers of ICIs have been reported, including the expression of PD-L1, tumor mutation burden, and tumor-infiltrating lymphocytes (TILs).[10-12] However, these biomarkers require tumor tissue samples collected by a biopsy. Noninvasive biomarkers have also been investigated in order to predict the clinical outcome of ICI therapy, including serum cytokines, soluble PD-L1, circulating tumor cells, and peripheral blood immune cells.[13-17] In NSCLC patients, changes in the serum levels of CXCL8 were identified as a biomarker of the response to anti-PD-1 Ab,[18] and an early increase in interleukin (IL)-6 after PD-1 blockade was reported to correlate with a better clinical outcome.[19] However, circulating biomarkers that might predict the efficacy of ICIs before the treatment has been initiated have yet to be identified in clinical practice.

Programmed death ligand 1 has been proposed to also be expressed by vessel endothelial cells.[20] Tumor angiogenesis is an essential mechanism involved in tumor progression by avoiding hypoxia.[21,22] In addition, several studies have revealed that tumor angiogenesis modifies tumor immunity by inhibiting the infiltration of antitumor immune cells, recruiting regulatory T cells and suppressing the maturation of immune cells.[23,24] However, the effects of PD-1/PD-L1 blockade on tumor angiogenesis remain unclear.

In the present study, we hypothesized that the molecular mechanisms underlying the regulation of the antitumor effect of PD-1/PD-L1 blockade have yet to be fully clarified and examined tumor angiogenesis.

2 | MATERIALS AND METHODS

2.1 | Cell lines

The mouse malignant pleural mesothelioma (MPM) cell line AB1-HA, a transfectant with the gene encoding influenza HA into AB1 cells, the mouse MPM cell line AC29, and the mouse squamous cell lung carcinoma cell line KLN205 were purchased from Public Health England. The mouse lung cancer cell line Lewis lung carcinoma (3LL), 293FT producer cells for production of lentiviral particle, and mouse vessel endothelial cell line MS-1 were purchased from ATCC. The mouse fibrosarcoma cell line MCA205 and mouse colon carcinoma cell line MC38 were generously provided by Dr SA Rosenberg (NCI, NIH). AB1-HA and 293FT were maintained in DMEM supplemented with 10% heat-inactivated FBS, penicillin (100 U/mL), and streptomycin (50 μg/mL). KLN205 was maintained in E-MEM with 10% FBS and 1% nonessential amino acids. The other cell lines were maintained in RPMI-1640 medium. All cells were cultured at 37°C in a humidified atmosphere of 5% CO_2 in air.

2.2 | Reagents

Anti-PD-L1 (clone 10F.9G2), anti-PD-1 (clone RMP1-14), and CXCR3-neutralizing (clone CXCR3-173) Abs were purchased from BioXCell. Isotype control IgG (rat IgG1, rat IgG2a, and hamster IgG) were also purchased from BioXCell.

2.3 | Animals

Six-week-old male BALB/c mice, athymic BALB/c nude mice, CBA/J mice, DBA/2 mice, and C57BL/6 mice were obtained from Charles River Japan Inc. All experiments were carried out in accordance with the guidelines established by the Tokushima University Committee on Animal Care and Use. At the end of each in vivo experiment, the mice were anesthetized with isoflurane and killed humanely by cutting the subclavian artery. All experimental protocols were reviewed and approved by the animal research committee of The University of Tokushima, Japan.

2.4 | In vivo subcutaneous implantation models of mouse tumor cells

AB1-HA cells (1.0×10^6 cells per mouse) suspended in 0.1 mL PBS were subcutaneously inoculated to the right flank of BALB/c mice or athymic BALB/c nude mice. 3LL, MC38, and MCA205 cells (1.0×10^6 cells per mouse) were subcutaneously inoculated to C57BL/6 mice. KLN205 (1.0×10^6 cells per mouse) and AC29 cells (2.0×10^6 cells per mouse) were subcutaneously inoculated to DBA/2 and CBA/J mice, respectively. The tumor size was measured using Vernier calipers twice a week, where volume $= ab^2\, 2^{-1}$ (a, long diameter; b, short diameter).

To determine the effect of PD-1/PD-L1 blockade on tumor growth, the mice were treated twice a week with anti-PD-L1 Ab (5 mg per kg per mouse), anti-PD-1 Ab (200 μg per mouse) or isotype control IgG by intraperitoneal injection from day 7 until they became moribund. The mice were killed humanely, and the tumors were resected for further analyses on days 14 and 21. To examine the effects of combination treatment with anti-PD-L1 Ab and anti-CXCR3 Ab, the mice were treated twice a week with 200 μg per mouse anti-CXCR3 Ab or isotype control IgG by intraperitoneal injection from day 7 (early treatment) or day 14 (late treatment) in addition to anti-PD-L1 Ab treatment.

2.5 | Immunohistochemical studies of mouse tumor tissue

The excised tumor tissues from the model mice were placed into OCT compound (Sakura Finetechnical Co.) and snap-frozen. Frozen tissue sections (8 μm thick) of tumors were fixed with 4% paraformaldehyde solution in PBS. To detect endothelial cells, rat anti-CD31/

PECAM-1 mAb (1:100, MEC 13.3; BD Pharmingen) was used. To assess hypoxia of tumor tissue, rabbit anti-CA9 polyclonal Ab (1:1000; Novus Biologicals) was used. Appropriate secondary Abs conjugated with peroxidase (ready to use, Nichirei) and the DAB Liquid System (Dako) were used to detect immunostaining. Nuclei were counterstained with hematoxylin (Dako). The number of CD31$^+$ vessel structures per field was evaluated at 200× magnification. One vessel structure stained with CD31$^+$ was counted as one regardless of the thickness or length. The immature vessels without lumens were excluded from the number of vessels. The number of total CD31$^+$ cells contained the number of both tumor vessels and immature vessels. The CA9-positive areas were calculated using the ImageJ software program (NIH) at 200× magnification. Images were acquired using a Keyence BZ-9000 microscope.

2.6 | Immunofluorescence of mouse tumor tissues

Frozen tissue sections (8 μm thick) were fixed with 4% paraformaldehyde solution in PBS and used for the identification of CD8$^+$ and CD4$^+$ T cells using a rat anti-CD8a mAb (1:150, 53-6.7; BD Pharmingen) and a rat anti-mouse CD4 (1:150, H129.19; BD Pharmingen), respectively. Anti-interferon-γ (IFN-γ) Ab and rabbit polyclonal Ab (1:50; Abcam) were used to examine the localization of IFN-γ. A rat anti-CD31/PECAM-1 mAb (1:150, MEC 13.3; BD Pharmingen), rabbit anti-collagen IV polyclonal Ab (1:400; Abcam), and rabbit anti-NG2 polyclonal Ab (1:150; Millipore) were used to detect endothelial cells, basement membrane, and pericytes, respectively. A rabbit anti-TIM-3 mAb (1:200, D3M9R; Cell Signaling Technology) was used to detect exhausted T cells. Alexa488- and Alexa594-labeled secondary Abs (1:250; Invitrogen) were used for immunofluorescent detection. Nuclei were counter-stained with DAPI (blue). In each slide, the number of positive cells was counted under a fluorescent microscope at 200× magnification. The pericyte coverage of the tumor vasculature was determined by double staining for CD31 and NG-2. These images were acquired using an Olympus BX61 fluorescence light microscope.

2.7 | Tissue clearing and 3D immunofluorescence

Tumor tissue clearing was undertaken with the CUBIC protocol.[25] We prepared ~1 cm^3 blocks of tumor tissue derived from MCA205 bearing mice treated twice a week with anti-PD-L1 Ab (5 mg per kg per mouse) or isotype control IgG on day 21. Tumor tissue were fixed with 4% paraformaldehyde solution in PBS for 24 hours before clearing. After washing in PBS, tumor tissue was delipidated with CUBIC-L (Tokyo Chemical Industry) with shaking for 4 days at 37°C. The CUBIC-L was refreshed every 2 days during the delipidation. For 3D staining of tumor vessels, the delipidated tissues were incubated with rat anti-CD31/PECAM-1 mAb (1:100, MEC 13.3; BD Pharmingen) in PBST with shaking for 3 days at 37°C. After washing in PBST, tumor tissue was stained with Alexa488-labeled secondary

Abs (1:100; Invitrogen) in PBST for 2 days at 37°C. The 3D stained tumor tissue was fixed with 1% paraformaldehyde solution in PBS for 3 hours at room temperature. Tumor tissue was refractory index-matched with CUBIC-R+ (Tokyo Chemical Industry). The sample was first incubated in 1:1 water-diluted CUBIC-R+ at room temperature with shaking overnight. The sample was then immersed in nondiluted CUBIC-R+ at room temperature for 24 hours. The 3D stained and cleared samples were mounted for imaging on 35-mm glass bottom dishes (Matsunami Glass) with mounting solution (Tokyo Chemical Industry). The 3D imaging was carried out using a confocal microscope (A1R; Nikon) equipped with diode lasers (405 and 488 nm; Coherent) and a 10× Objective (PlanApo λ, NA 0.45, WD 4 mm). Optical slices for a part of the cleared samples (XY: 984 × 984 μm, Z: 230 μm) were collected with a 2× scan zooming at a 10-μm interval (Z), then reconstructed using the NIES elements software (Nikon).

2.8 | Quantitative RT-PCR

Tumor cell lines (3×10^5 cells per 2 mL) were each plated into 6-well plates (BD Biosciences) in 10% FBS containing DMEM and incubated for 24 hours. The culture medium was then changed to fresh medium with or without recombinant mouse IFN-γ protein (20 ng/mL; PeproTech), after which the cells were incubated for an additional 48 hours. Total RNA was extracted from the tumor cell lines or tissue using the RNeasy Mini Kit (Qiagen) and reverse-transcribed to cDNA using a High Capacity cDNA Reverse Transcription Kit (Applied Biosystems). The RT-PCR was carried out using the CFX96 real-time PCR system (Bio-Rad) or SYBR Premix Ex Taq (Takara). Mouse _RPS29_ mRNA was used as a housekeeping gene, and quantification was performed using the ΔΔCt method. The specific PCR primer pairs used for each studied gene are shown in Table S1.

2.9 | Detection of protein expression in serum of tumor-bearing mice

To collect serum from AB1-HA or KLN205 tumor-bearing mice, the mice were anesthetized with isoflurane. Whole blood was collected from the heart using a 27-G needle with a 1-mL syringe and incubated overnight at 4°C, then centrifuged at 20 _g_ for 10 minutes. The supernatant was transferred and stocked as serum. Serum from tumor-bearing mice was used to detect the concentrations of mouse CXCL9, CXCL10, and CXCL11 using ELISA kits (Abcam).

2.10 | Detection of protein expression in serum of NSCLC patients

Serum from 17 NSCLC patients were provided by The University of Tokushima. Informed consent was obtained from all patients, and the protocol was approved by the Institutional Review Board of Tokushima University Hospital (No. 2924). Whole human blood

was centrifuged at 210 g for 10 minutes. The supernatant was transferred and stocked as serum. Serum from NSCLC patients were used to detect the concentrations of human CXCL9, CXCL10, and CXCL11 using ELISA kits (Abcam) according to the manufacturer's instructions.

2.11 | Cell proliferation assays of mouse vessel endothelial cells

MS-1 mouse vessel endothelial cells (2×10^3 cells per 100 μL) were plated into each well of a 96-well plate (BD Biosciences) in 10% FBS containing RPMI-1640 and incubated for 24 hours. Anti-PD-L1 Ab or anti-PD-1 Ab (0.004-12.5 μg/mL) was then added, and the cells were incubated for an additional 72 hours. The proliferation of MS-1 was measured using the MTT dye reduction method. The absorbance was measured with a SUNRISE Remote R microplate reader (Tecan).

2.12 | Flow cytometry

To examine the surface expression of PD-L1 and IFN-γ receptor 1 (IFNGR1) in mouse tumor cell lines, phycoerythrin-conjugated Abs to CD274 (PD-L1, 1:50, MIH5; eBioscience) and CD119 (IFNGR1, 1:50, 2E2; eBioscience) were used. The stained cells were analyzed by flow cytometry using a BD LSRFortessa (BD Bioscience) for acquisition and the FlowJo software program (Tree Star) for the analysis.

2.13 | Transfection of lentiviral shRNA

Lentiviral shRNA pLKO.1 constructs (Horizon) were used to make self-inactivating shRNA lentivirus for NM_019494 CXCL11 (TRCN0000068243), and a nontarget random scrambled sequence control. To harvest the lentiviral particles, shRNA was cotransfected with MISSION Lentiviral Packaging Mix (Sigma-Aldrich) in packaging cells (293FT) by using FuGENE 6 (Roche). For virus transduction, 2.0×10^6 AB1-HA cells were incubated with lentivirus containing 5 μg/mL polybrene (Chemicon International) for 24 hours. The successfully transduced clones were identified by puromycin (Sigma-Aldrich) selection.

2.14 | Statistical analyses

Data are presented as the mean ± SEM. The statistical analyses were undertaken using Student's t test for unpaired samples, the Mann-Whitney U test or a one-way ANOVA, followed by Tukey's multiple comparison post-hoc test, as appropriate. The correlation was estimated by Pearson's correlation and a linear regression analysis. P values of less than .05 were considered to be statistically significant.

3 | RESULTS

3.1 | Antiangiogenic effects of PD-1/PD-L1 blockade in a mouse model

Initially, to investigate the efficacy of anti-PD-L1 Ab, we subcutaneously injected syngeneic mice with various types of malignant mouse cell lines. Seven days after tumor injection, anti-PD-L1 Ab was given twice a week for two weeks. Anti-PD-L1 Ab showed an antitumor effect in AB1-HA, MCA205, MC-38, and AC-29 cell lines compared to the control IgG (Figures 1A and S1). In contrast, PD-L1 blockade had no effect on the tumor progression in KLN205- and 3LL-bearing mice (Figures 1B and S1).

To investigate the relationship between the antitumor effects of anti-PD-L1 Ab and tumor angiogenesis, tumors were harvested at the end-points, and the tumor microvessels were immunohistochemically evaluated.[26,27] Interestingly, the tumor microvessels were significantly reduced by PD-L1 blockade in treatment-sensitive tumor tissues AB1-HA and MCA205, whereas the number of clustered CD31^{+} endothelial cells was significantly increased (Figures 1C,D and S2A,B). The same result was confirmed by administering anti-PD-1 Ab (Figure S3). These clustered endothelial cells did not form the vessel lumen; however, they had a collagen IV^{+} basement membrane and pericyte coverage (Figure S4). These findings indicate that clustered CD31^{+} endothelial cells had features of immature angiogenic vessels. This "immature angiogenesis" was not observed in PD-L1 blockade-resistant tumor tissues, namely KLN-205 and 3LL. To investigate the effect of PD-L1 blockade in tumor vascular structure, hydrophilic tissue-clearing and 3D imaging of CD31^{+} endothelial cells were undertaken in MCA205 tumor tissue (Figure 1E). Notably, the vascular formations were obviously inhibited by PD-L1 blockade, and the accumulation of clustered CD31^{+} endothelial cells was observed.

Furthermore, anti-PD-L1 Ab induced unique net-like hypoxia only in ICI-sensitive tumor tissues (Figures 2 and S2C,D). These results suggest that the angiostatic effects by PD-1/PD-L1 blockade were universally observed in relation to treatment sensitivity.
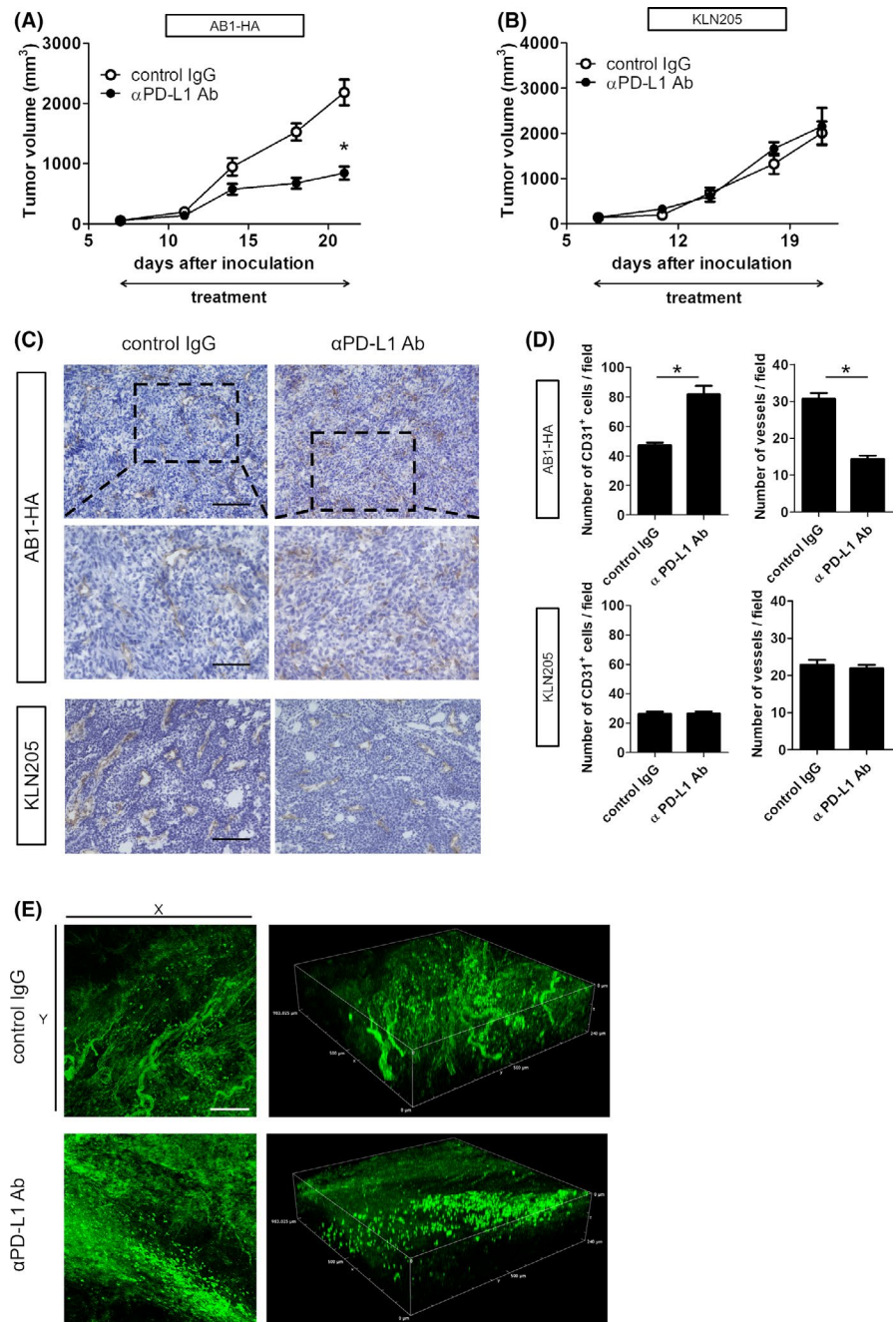
3.2 | Angiostatic effects of PD-L1 blockade and the need for T cell function

To determine the mechanisms by which PD-1/PD-L1 blockade regulates tumor angiogenesis, we examined the direct effect of anti-PD-1/PD-L1 Ab on the proliferation of mouse vessel endothelial cells in vitro (Figure S5). The proliferation of vessel endothelial cells was not suppressed by anti-PD-1/PD-L1 Ab in vitro, suggesting that the antiangiogenic effects of PD-1/PD-L1 blockade work through an indirect process in the tumor microenvironment.

We then examined the antiangiogenic effects of PD-L1 blockade in AB1-HA tumor-bearing BALB/c nude mice to determine whether T cell activity contributes to the angiogenesis (Figure 3). Anti-PD-L1 Ab exerted no significant effects on tumor progression

FIGURE 1 Treatment with programmed death ligand 1 (PD-L1) Ab inhibits tumor angiogenesis in vivo. The evaluation of the tumor volume of (A) AB1-HA and (B) KLN205 tumor-bearing mice treated with anti-PD-L1 Ab (αPD-L1 Ab) beginning 7 d after tumor cell injection. C, Representative images of sections from AB1-HA and KLN205 tumors stained for CD31. The tumors were harvested at day 21 from the control and αPD-L1 Ab-treated groups. Scale bar, 200 μm. D, Quantitative evaluation of the total number of CD31$^+$ cells and vessel structures per field in each tumor of mice (n = 7 per group) studied in (C). E, Reconstructed 3D images of cleared MCA205 tumors stained for CD31. Tumors were harvested at day 21 from the control and αPD-L1 Ab-treated groups. 3D-stained tumors were imaged with confocal microscopy (z-stack: 240 μm/24 slices). 3D view images (right) and x-y plane maximum intensity projection images (left) are presented. Scale bar, 200 μm. Data are shown as mean ± SEM. *P < .05, Mann-Whitney U test


or angiogenesis in tumor-bearing nude mice lacking mature T cells. These results indicate that the angiostatic effect of PD-1/PD-L1 blockade requires the T cell function.

## 3.3 | Effect of PD-L1 blockade on CXCL10/11 expression in treatment-sensitive tumors

To identify the molecules that contribute to the angiostatic effects of anti-PD-1/PD-L1 therapy, we examined the gene expression of various angiogenic or angiostatic molecules in mouse tumor tissue treated with anti-PD-L1 Ab by undertaking a quantitative PCR analysis. The expression of angiogenesis-related molecules was examined

on day 14 after tumor cell (AB1-HA and KLN205) inoculation, and a more than two-fold upregulation of mouse *Ifng* and *Cxcl9/10/11* was observed in PD-L1 blockade-treated AB1-HA (PD-L1 blockade-sensitive cell line) tumor tissue (Figure 4A). However, the expression of mouse *Cxcl10/11* was not changed by anti-PD-L1 Ab when the KLN205 (PD-L1 blockade-resistant cell line) tumor tissue was examined (Figure 4B).

The CXCL9/10/11 CXC chemokines lack an ELR (Glu-Leu-Arg) motif and are secreted in response to IFN-γ.[28] The CXCL9/10/11 and receptor CXCR3 axis has been reported to regulate various tumor microenvironment cells, enhancing the migration of lymphocytes and suppressing tumor angiogenesis.[28,29] As the gene expression of *CXCL10/11* was increased only in the tumor tissue against which
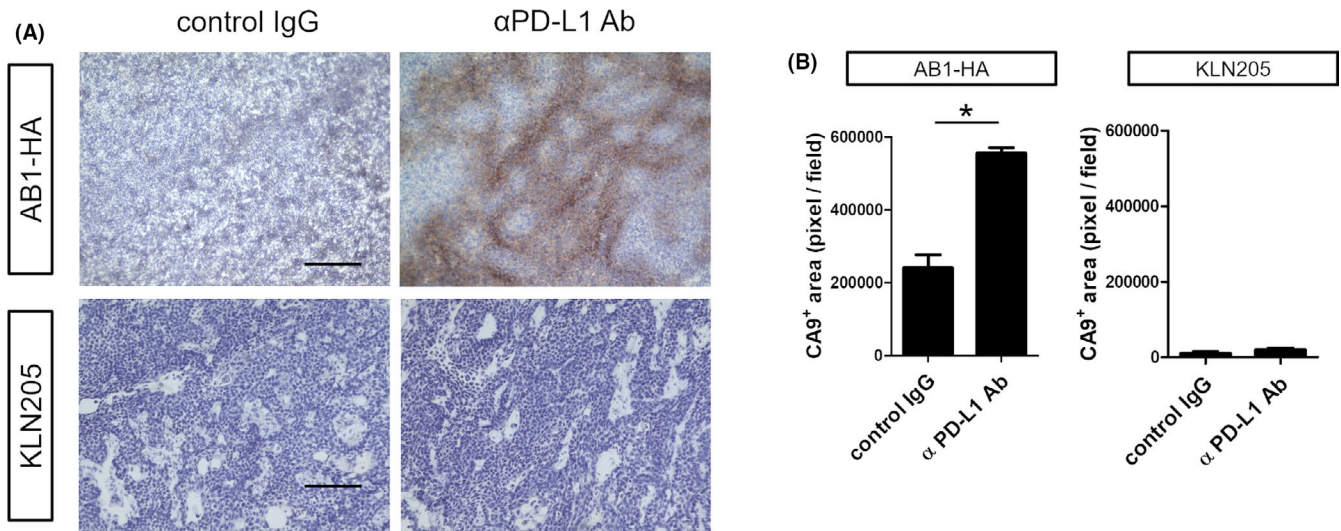
FIGURE 2 Treatment with programmed death ligand 1 (PD-L1) Ab induces tumor hypoxia. A, Representative images of sections from AB1-HA and KLN205 tumors stained for CA9. The tumors were harvested at day 21 from the control and αPD-L1 Ab-treated groups. Scale bar, 200 μm. B, Evaluation of the CA9-positive area (n = 7 per group). Data are shown as mean ± SEM. *$P < .05$, Mann-Whitney U test
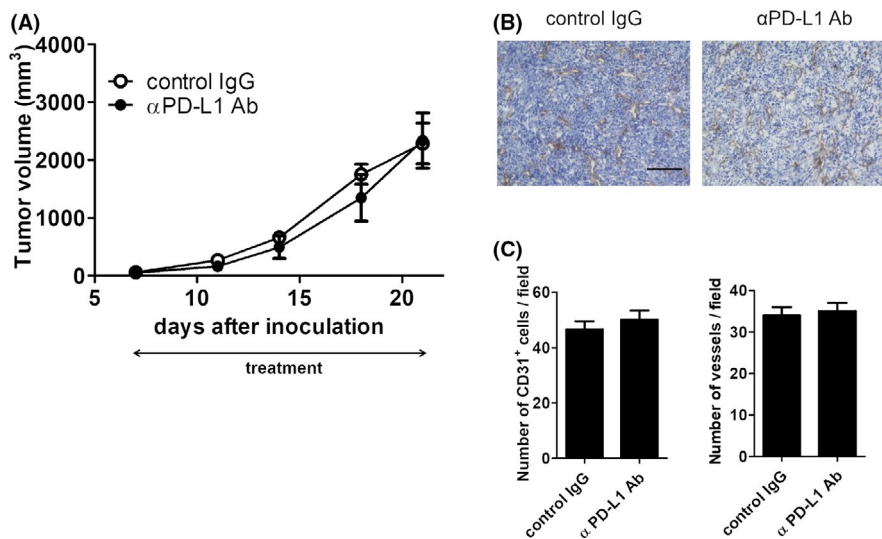

FIGURE 3 T cells are required in the antiangiogenic effects of programmed death ligand 1 (PD-L1) blockade. A, Evaluation of the tumor volume of AB1-HA tumor-bearing BALB/c nude mice treated with αPD-L1 Ab beginning from 7 d after tumor cell injection. B, Representative images of sections from AB1-HA tumors stained for CD31. Tumors were harvested at day 21 from the control and αPD-L1 Ab-treated BALB/c nude mice. Scale bar, 200 μm. C, Quantitative evaluation of the total number of CD31^{+} cells and vessel structures per field in each tumor of mice (n = 7 per group) studied in (B). *$P < .01$, Mann-Whitney U test. All data are shown as mean ± SEM

PD-L1 blockade showed antitumor and antiangiogenic effects, we focused on CXCL10/11 as candidate molecules for modulating the sensitivity to anti-PD-1/PD-L1 therapy and confirmed that the protein expression of mouse CXCL10 was significantly increased and that of CXCL11 showed an increasing trend in the serum of PD-L1 blockade-treated AB1-HA tumor-bearing mice (Figure 4C). Mouse CXCL9 was also significantly increased in the serum of PD-L1 blockade-treated AB1-HA tumor-bearing mice. In contrast, an increase in serum CXCL9 protein was also detected in PD-L1 blockade-treated KLN205 tumor-bearing mice, whereas the serum

levels of CXCL10 and CXCL11 were not changed (Figure 4D). These results suggest that CXCL10/11 but not CXCL9 have potential utility as key modulators of the antitumor and antiangiogenesis effects of PD-1/PD-L1 blockade and as circulating biomarkers predicting drug sensitivity.

In addition, the concentration of serum CXCL10 was higher in AB1-HA tumor-bearing mice without PD-L1 blockade than in KLN205 tumor-bearing mice (Figure 4C,D), indicating that the concentration of angiostatic chemokines in pretreatment serum correlates with the outcome of immune checkpoint blockade.
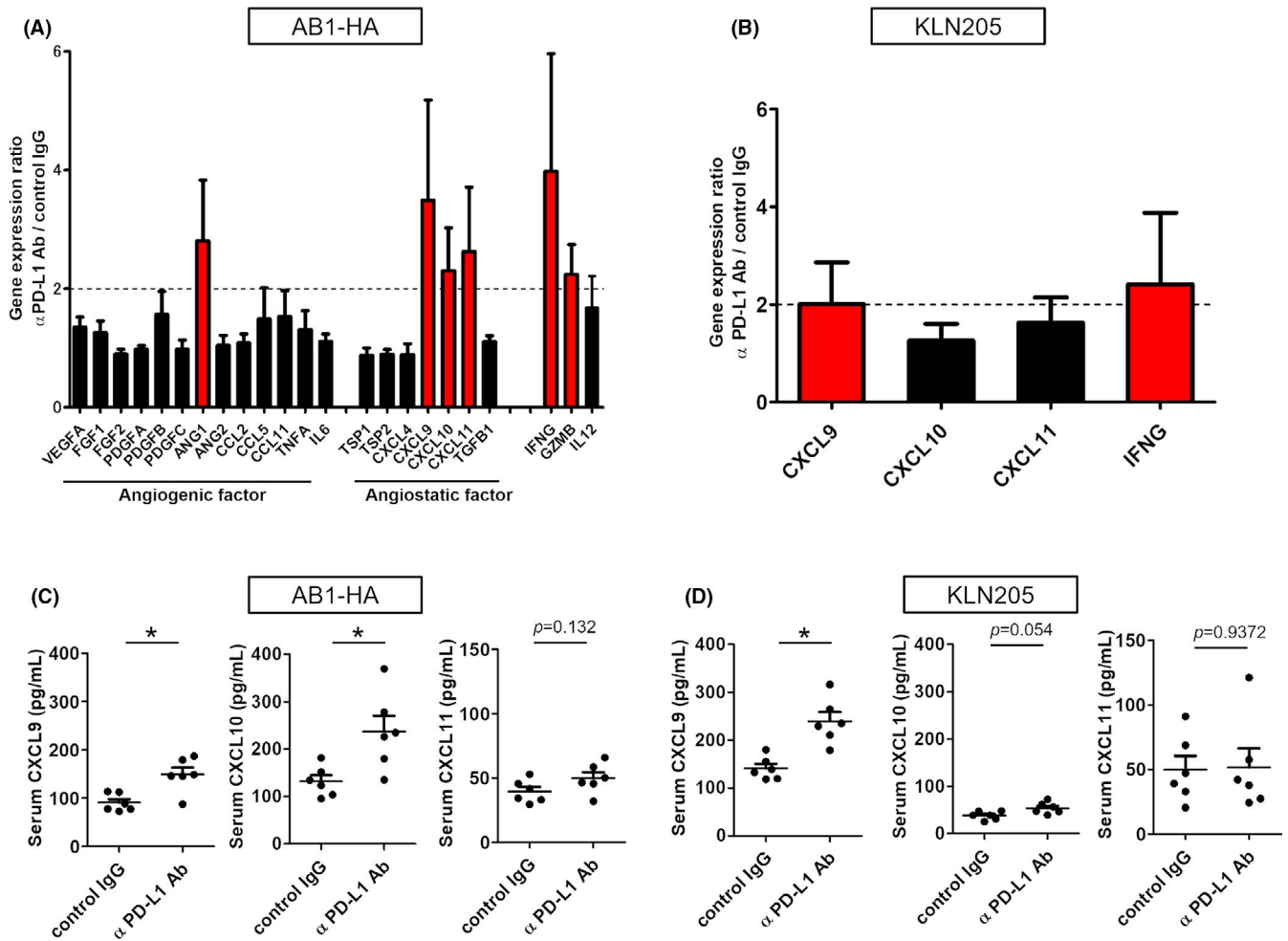
FIGURE 4 Identification of CXCL10/11 as the angiostatic factors induced by treatment with anti-programmed death ligand 1 (PD-L1) Ab. A, Comparison of mouse mRNA expression of proangiogenic factors and angiostatic factors in subcutaneous AB1-HA tumors treated with or without anti-PD-L1 Ab (αPD-L1 Ab) at day 14 after tumor inoculation. Fold-changes in the mRNA expression of the αPD-L1 Ab-treated tumors compared with control tumors are shown. Genes upregulated more than two-fold in αPD-L1 Ab-treated mice compared with the control group are shown as red columns. B, Comparison of mouse mRNA expression of *CXCL9/10/11* and *IFNG* in the subcutaneous KLN205 tumors treated with or without anti-PD-L1 Ab (αPD-L1 Ab). C, D, Amounts of mouse CXCL9/10/11 measured by ELISA in serum from (C) AB1-HA and (D) KLN205 tumor-bearing mice treated with or without αPD-L1 Ab (n = 6 per group). Data are shown as mean $\pm$ SEM. *$P < .05$, Mann-Whitney U test. ANG, angiopoietin; FGF, fibroblast growth factor; GZM, granzyme; IFN, interferon; IL, interleukin; PDGF, platelet-derived growth factor; TGF, transforming growth factor; TNF, tumor necrosis factor; TSP, thrombospondin; VEGF, vascular endothelial growth factor

r=0.2066, p=0.3962 r=0.5311, p=0.0283 r=0.5473, p=0.0230
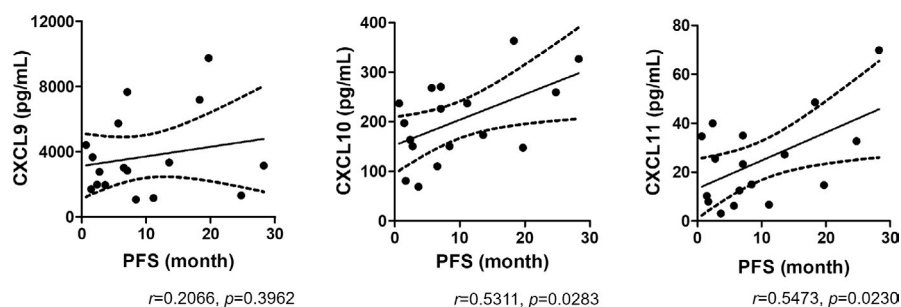
FIGURE 5 Predictive utility of serum CXCL10/11 levels for the clinical outcome of non-small-cell lung cancer (NSCLC) patients treated with anti-programmed death 1 (PD-1) Ab. The pretreatment amount of human CXCL9/10/11 measured by ELISA in the serum from 17 NSCLC patients who received anti-PD-1 Ab (pembrolizumab). Correlation of serum concentrations of CXCL9/10/11 and progression-free survival (PFS) of patients was analyzed. The correlation was estimated by Pearson's correlation and a linear regression analysis (best-fit line is indicated together with 95% confidence bands)

3.4 | Correlation of the serum concentration of CXCL10/11 with clinical outcome in human lung cancer patients who received anti-PD-1 Ab

To determine whether serum angiostatic chemokines contribute to the clinical outcome of ICI therapy, we examined the concentration of CXCL9/10/11 protein in the pretreatment serum of 17 NSCLC patients receiving first-line treatment with the anti-PD-1 Ab pembrolizumab.[10]

The patients' characteristics are summarized in Table S2. The correlation between the concentration of serum angiostatic chemokines and progression-free survival (PFS) was analyzed. The serum concentration of CXCL10/11 in the pretreated NSCLC patients was significantly correlated with the clinical outcome of first-line pembrolizumab treatment (Figure 5). In contrast, serum CXCL9 did not significantly affect the PFS in NSCLC patients treated with pembrolizumab.

Taken together, these findings suggest that serum CXCL10/11 have potential utility as circulating biomarkers predicting the clinical outcome of anti-PD-1 therapy in NSCLC patients.

3.5 | Relevance of *CXCL10/11* gene expression and ICI sensitivity in tumor cells

We next examined whether tumor cells are the main source of CXCL10/11 in response to ICI therapy. In our previous reports, PD-1 blockade induced IFN-γ expression in TILs in AB1-HA tumor-bearing mice.[30] In the present study, we also showed that IFN-γ was specifically expressed in CD4^{+} or CD8^{+} TILs in AB1-HA tumor-bearing mice treated with PD-L1 blockade (Figure S6). Thus, as we observed that PD-L1 blockade did not affect tumor angiogenesis in BALB/c nude mice, there was a possibility that the expression of angiostatic chemokines would be induced by T cell-derived IFN-γ. To confirm this, we examined the gene expression of *Cxcl9/10/11* and *PD-L1* in each mouse tumor cell line with or without mouse IFN-γ protein.

The relationships between the expression of angiostatic chemokines and the sensitivity to anti-PD-L1 Ab were investigated in vitro (Figure 6). Mouse *Cxcl10/11* were upregulated by IFN-γ only in the PD-L1 blockade-sensitive tumor cell lines (Figure 6B,C). *Cxcl9* was also upregulated in some tumor cell lines that showed sensitivity to anti-PD-L1 Ab, but MCA205 did not show any *Cxcl9* upregulation in the IFN-γ stimulation (Figure 6A). In addition, *Cxcl9* levels were increased in 3LL cells, which are resistant to anti-PD-L1 Ab, in vivo. Because the expression level of PD-L1 in tumor tissue have been used to predict the clinical outcome of anti-PD-1/PD-L1 Ab,[10-12] the PD-L1 expression was examined in mouse tumor cell lines (Figures 6D and S7). In tumor cells, the gene and cell surface expression of PD-L1 were not essential in the sensitivity to PD-L1 blockade in vivo. Considering the expressions of CXCL10/11 were induced by IFN-γ, the correlations with the IFNGR expression in tumor cells and the sensitivity to PD-L1 blockade were examined (Figure S7). All the cell lines that showed the sensitivity to IFN-γ expressed IFNGR1.

The IFNGR expression in tumor cells could be essential for the sensitivity against IFN-γ and anti-PD-L1 Ab.

These results indicate that tumor cell-derived CXCL10/11 were related to the antitumor effects of PD-1/PD-L1 blockade, and these angiostatic chemokines were regulated by IFN-γ.

3.6 | Influence of CXCR3 blockade on angiostatic effect of PD-L1 Ab in a mouse model

To verify the importance of the CXCL10/11-CXCR3 axis in the antitumor and antiangiogenic effects of the PD-1/PD-L1 blockade in vivo, AB1-HA tumor-bearing mice were treated with anti-PD-L1 Ab and/or anti-CXCR3 Ab. In recent studies, the CXCL9/10-CXCR3 axis was reported to play an essential role in ICI treatment by recruiting CXCR3^{+} T cells.[31-33] Therefore, in order to examine the antitumor mechanisms of the CXCL10/11-CXCR3 axis, except for the T cell recruitment, we compared the efficacy between anti-CXCR3 Ab early (days 7-21) and late (days 14-21) administration after tumor inoculation. Anti-CXCR3 Ab inhibited the antitumor effects of anti-PD-L1 Ab both in the early and late treatment groups (Figure 7A). However, the T cell recruitment via PD-L1 blockade was inhibited only in combination with the early treatment of anti-CXCR3 Ab (Figure 7B,C). To examine the exhaustion of TILs, we undertook double-staining of TIM-3 and CD8 in AB1-HA tumor tissue treated with anti-PD-L1 Ab (days 7-21) and anti-CXCR3 Ab (days 14-21) (Figure S8). The percentages of exhausted T cells were not increased by CXCR3 blockade. These results suggest that the antitumor effect of anti-PD-L1 Ab is regulated by a mechanism other than T cell recruitment in the late phase of treatment.

To test this hypothesis, we analyzed the angiogenesis in the tumor tissue of anti-PD-L1 and/or anti-CXCR3 Ab-treated mice by immunohistochemistry (Figure 7D,E). The number of mature vessels was decreased in mice treated with anti-PD-L1 Ab monotherapy. However, anti-CXCR3 Ab reversed the angiostatic effects of anti-PD-L1 Ab in both early- and late-phase treatment. In addition, the hypoxic area (CA9^{+} area) induced by PD-L1 blockade also recovered following both early and late treatment with anti-CXCR3 Ab (Figure 7F,G). Considering the effect of different duration (early, days 7-21; late, days 14-21) of CXCR3 blockade, we also undertook combination therapy with anti-PD-L1 Ab (days 7-21) and anti-CXCR3 Ab (days 7-14) (Figure S9). Blockade of CXCR3 (days 7-14) also inhibited the antitumor effects, T cell recruitment, and angiostatic effect of anti-PD-L1 Ab as with the longer term treatment (days 7-21). Taken together with the results from human NSCLC patients, these findings suggest that the CXCL10/11-CXCR3 axis might be a key modulator of the antitumor effect of PD-1/PD-L1 blockade by suppressing tumor angiogenesis.

3.7 | Effect of CXCL11 silencing in tumor cells following PD-L1 Ab treatment in a mouse model

The present study showed that angiostatic chemokines were mainly secreted from tumor cells exposed to IFN-γ. In contrast, recent
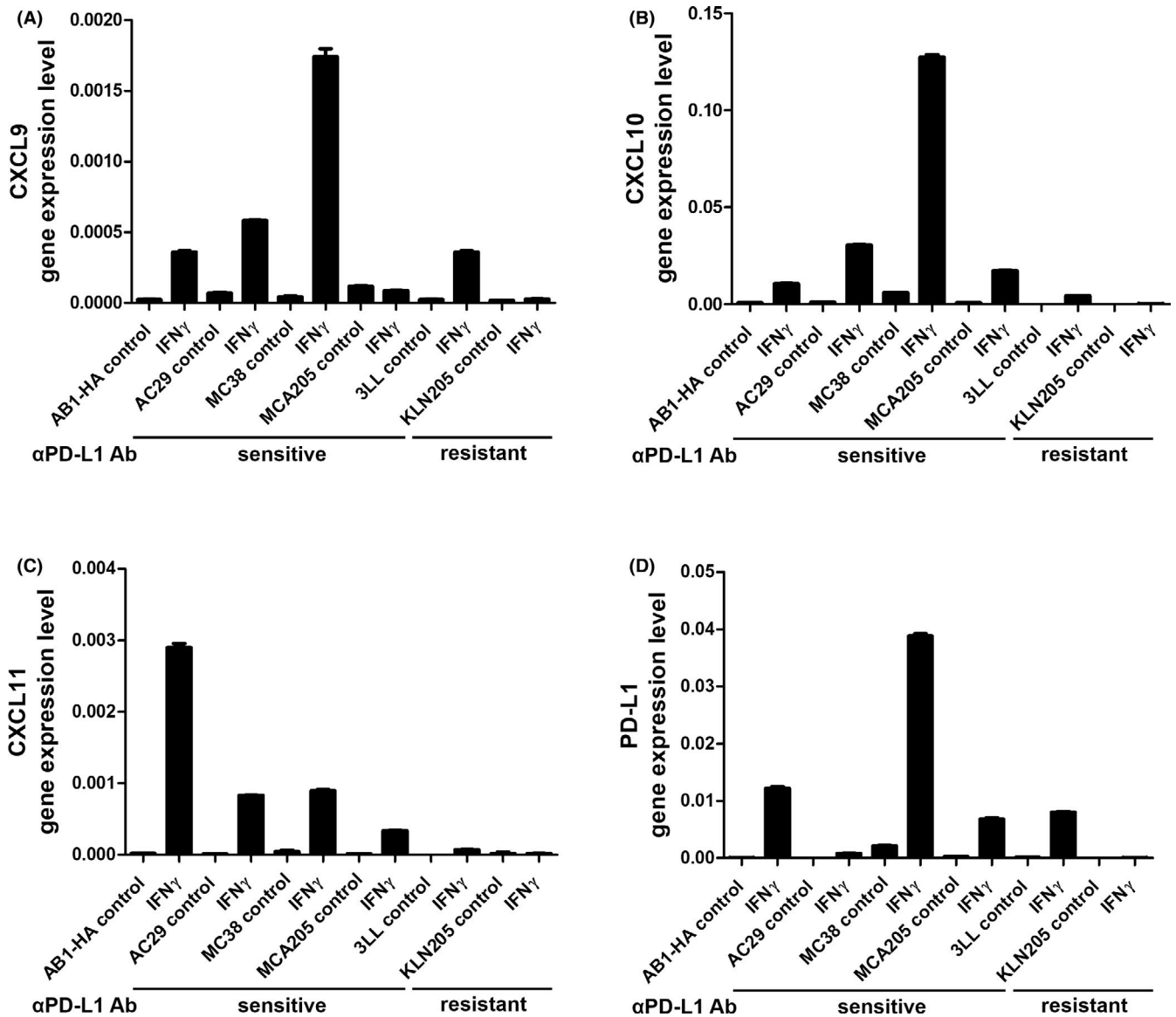
FIGURE 6 Identification of tumor cell-derived CXCL10/11 as the prognostic factors of anti-programmed death ligand 1 Ab. A comparison of the mouse mRNA expression of (A) CXCL9, (B) CXCL10, (C) CXCL11, and (D) PD-L1 in mouse tumor cell lines with or without recombinant mouse γ-interferon (IFN-γ; 20 ng/mL) in vitro. Data are shown as mean ± SEM

studies indicated that tumor-infiltrating immune cells, such as macrophages and dendritic cells, also produced CXCL9/10 to recruit T cells.[32,33] Furthermore, the effects of CXCL11 in treatment with anti-PD-L1 Ab are still unclear, whereas CXCL9/10 were reported as the predictive biomarkers of ICI treatment.[33] To examine the importance of tumor-derived angiostatic chemokines in the antitumor effects of PD-L1 blockade, we established AB1-HA cells transfected with shRNA plasmid targeting CXCL11 (Figure 8A). We revealed that PD-L1 blockade did not suppress tumor progression in CXCL11 knock-down cells-bearing mice (Figure 8B). In addition, CXCL11 silencing in tumor cells also inhibited the angiostatic effects of PD-L1 blockade in vivo (Figure 8C,D). Hence, the present study revealed that tumor-derived angiostatic chemokines played a pivotal role in immunotherapy with PD-L1 blockade by regulating the angiogenesis.

4 | DISCUSSION

In the present study, we discovered that anti-PD-1/PD-L1 Ab inhibits tumor angiogenesis in vivo, and tumor cell-derived CXCL10/11 were identified as key molecules regulating the antiangiogenic effects of ICI. Notably, CXCL10/11 in serum of patients with lung cancer before treatment served as a potential biomarker for clinical response of ICI.

The immunohistochemical analysis of tumor microvessels clarified the angiostatic effects of ICI in this study. In ICI-responder tumors, the vessel lumen disappeared, and the vessel continuity was completely lost after ICI treatment, while the numbers of small clusters of CD31^{+} cells were increased. We regarded these clusters of endothelial cells as immature vessels without blood flow, because ICI treatment significantly induced tumor net-like
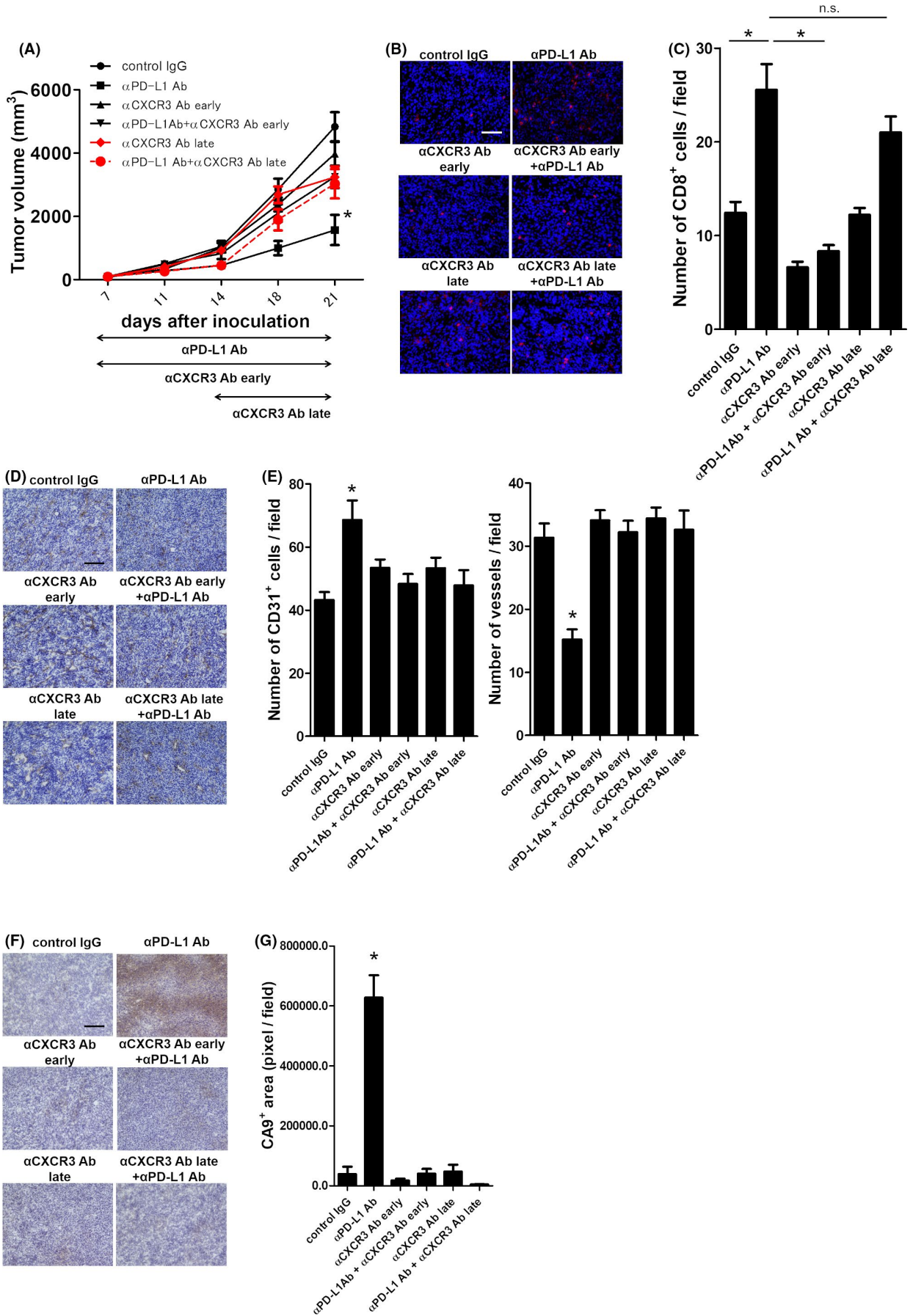
FIGURE 7 Involvement of the CXCL10/11-CXCR3 axis in angiogenesis through programmed death ligand 1 (PD-L1) blockade. The effect of CXCR3 inhibition in addition to anti-PD-L1 Ab (αPD-L1 Ab) treatment in vivo. A, Evaluation of the tumor volume of AB1-HA tumor-bearing mice treated with anti-PD-L1 Ab (αPD-L1 Ab) starting 7 d after tumor cell injection. Mice were treated with anti-CXCR3 Ab (αCXCR3 Ab) from 7 d (early treatment) or 14 d (late treatment) after tumor inoculation. B, Representative images of sections from AB1-HA tumors stained for CD8a. Tumors were harvested at day 21 from each group in (A). Scale bar, 200 μm. C, Quantitative evaluation of the total number of CD8a$^+$ cells in each tumor of mice (n = 7 per group) studied in (B). D, Representative images of sections from AB1-HA tumors stained for CD31. Tumors were harvested at day 21 from each group in (A). Scale bar, 200 μm. E, Quantitative evaluation of the total number of CD31$^+$ cells and vessel structures per field in each tumor of mice (n = 7 per group) studied in (D). F, Representative images of sections from AB1-HA tumors stained for CA9. Tumors were harvested at day 21 from each group in (A). Scale bar, 200 μm. G, Evaluation of the CA9-positive area (n = 7 per group). Data are shown as mean ± SEM. *P < .05, one-way ANOVA
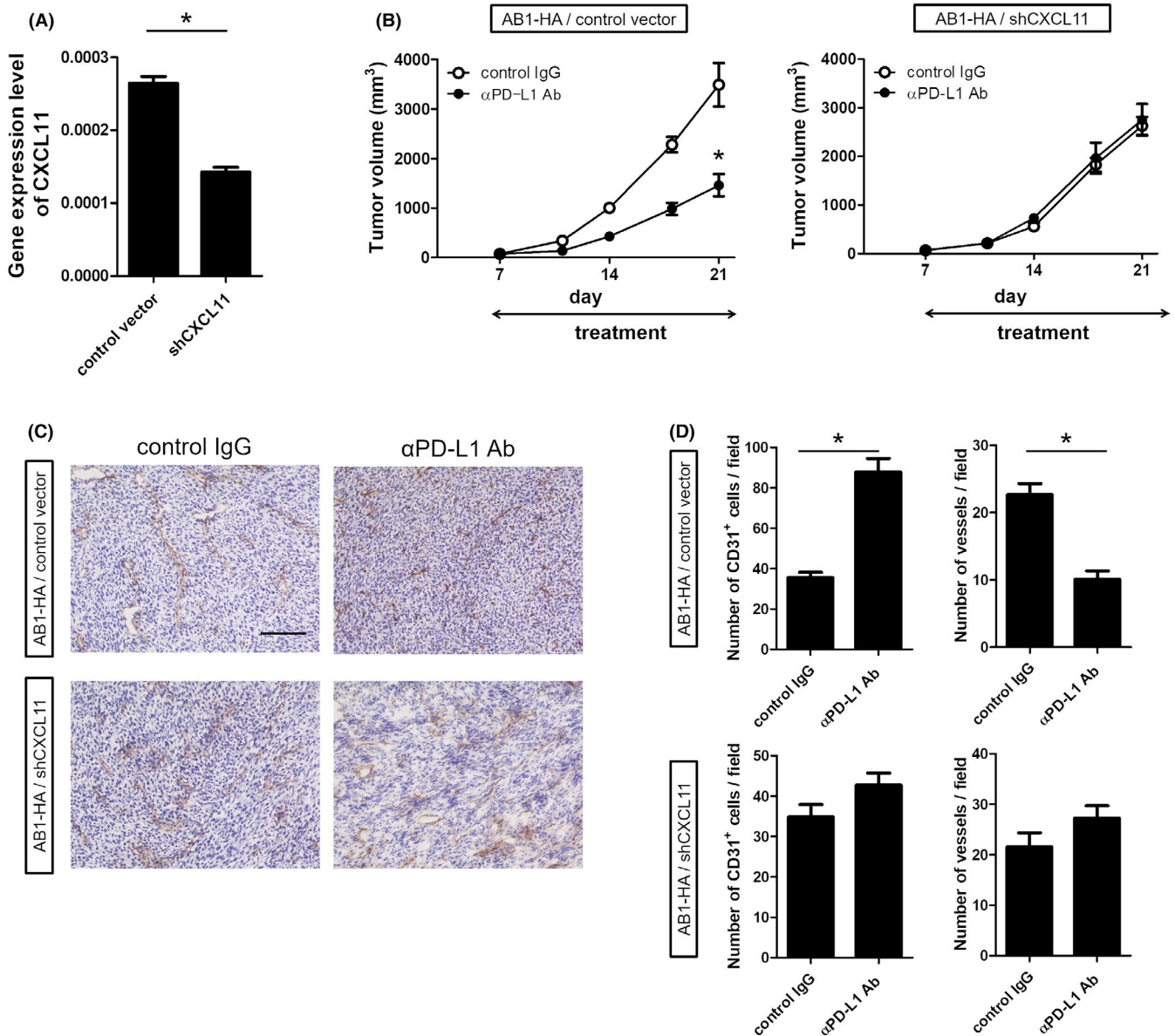
FIGURE 8 Effect of CXCL11 silencing in tumor cells on the treatment of programmed death ligand 1 (PD-L1) blockade. A, Comparison of mouse mRNA expression of CXCL11 in AB1-HA cells transfected with nontargeting control plasmid (AB1-HA/control vector) or CXCL11-targeting shRNA plasmid (AB1-HA/shCXCL11). Each cell was treated with mouse recombinant γ-interferon (20 ng/mL) for 24 h in vitro. B, Evaluation of tumor volumes of AB1-HA/control vector or shCXCL11 tumor-bearing mice treated with anti-PD-L1 Ab (αPD-L1 Ab) from seven days after tumor cell injection. C, Representative images of sections from AB1-HA/control vector or shCXCL11 tumors stained for CD31. Tumors were harvested at day 21 from each group in (B). Scale bar, 200 μm. D, Quantitative evaluation of the total number of CD31$^+$ cells and vessel structures per field in each tumor of mice (n = 8 per group) studied in (C). Data are shown as mean ± SEM. *P < .05, Mann-Whitney *U* test

hypoxia. The specific patterns of angiogenic networks have potential utility in predicting the outcome of ICI treatment, as with the PD-L1 expression and TILs in tumor tissue. In addition, recent studies have reported that the hypoxic condition enhances the cytotoxicity and cytokine producibility of T cells.[34-36] Therefore, the present study suggested that continuous treatment with ICI improves antitumor immunity by not only direct effects but also the indirect anti-angiogenic process.

The CXCL9/10/11 chemokines have been reported to influence the migration and activation of antitumor immune cells.[28] Gene transfection and CXCL9/10/11 protein administration were also reported to improve antitumor immunity.[37-39] Recent studies revealed that CXCL9/10 production from tumor-infiltrating CD103^{+} dendritic cells or macrophages were required for the antitumor effect of ICI by recruiting CXCR3^{+} T cells.[32,33]

However, CXCL9/10/11 are also known to have other aspects as antiangiogenic molecules. Feldman et al[40] reported that CXCL10 induces the apoptosis of vessel endothelial cells and inhibits tumor angiogenesis in vivo. Arenberg et al[41] revealed that continuous treatment with CXCL10 inhibits tumor progression and angiogenesis in tumor-bearing immunodeficient mice. Although IFN-inducible ELR[−] CXC chemokines have been known to contribute to both tumor immunity and angiogenesis, the angiostatic effects of ICI by regulating CXCL9/10/11 have not been clarified.

Among the angiostatic chemokines, we focused on tumor-derived CXCL10/11 in particular. The present study revealed that the expression levels of CXCL10/11, not CXCL9, in tumor cells or serum correlated with the antitumor effect of PD-1/PD-L1 blockade in mouse models and lung cancer patients. It is widely known that CXCL10 is a biomarker that can predict sensitivity to ICI[32,33] and its angiostatic effect has been proven. However, the roles of CXCL11 in tumor microenvironment is still unclear, compared with CXCL10. Therefore, we revealed that CXCL11 silencing in tumor cells suppressed the antitumor and angiostatic effects of PD-L1 blockade (Figure 8). Taken together, we showed the importance of tumor-derived CXCL11 in immunotherapy, as well as CXCL10.

Based on the results of combination treatment with anti-PD-L1 Ab and anti-CXCR3 Ab in a syngeneic mouse model (Figure 7), the early phase of ICI treatment was shown to require CD8^{+} T cell recruitment through the CXCL10/11-CXCR3 axis to suppress tumor progression, as in recent investigations.[31-33] However, the present results showed that CXCR3 blockade also inhibits the antitumor and angiostatic effects of ICI even after the recruitment of T cells. The efficacy of late-phase ICI treatment was thus presumed to depend on the antiangiogenic activity of CXCL10/11, not on the immune cell recruitment.

The present study indicated that the productivity of angiostatic chemokines and sensitivity to IFN-γ in tumor cells could have the potential to influence the clinical outcome of ICI treatment. Although all the cell lines that showed sensitivity to IFN-γ expressed IFNGR1, 3LL cells, which showed poor sensitivity to IFN-γ, also expressed IFNGR1 in the present study (Figure S7). Manguso et al found that the deletion of IFN-γ pathway-related molecules, such as IFNGR,

JAK1/2, and STAT1, induced resistance to anti-PD-1 therapy in tumor cells.[42] In melanoma patients, loss-of-function mutations in JAK1/2 were found to contribute to acquired resistance to anti-PD-1 treatment.[43] These mechanisms could regulate the production of angiostatic chemokines in IFNGR^{+} tumor cells in response to IFN-γ.

In our study, anti-PD-L1 Ab did not exert antiangiogenic effects in tumor-bearing BALB/c nude mice, which lack T cells (Figure 3). In addition, treatment with anti-PD-L1 Ab induced the upregulation of the IFNG gene in both ICI-sensitive and ICI-resistant cell lines, whereas CXCL10/11 were induced only in ICI-responder cells (Figure 6). Tumor-infiltrating lymphocytes are recognized as the main source of IFN-γ in the tumor microenvironment.[30] The present findings suggest that T cell-derived IFN-γ was essential for the upregulation of the CXCL10/11 expression in tumor tissue treated with ICIs. According to current knowledge, an increase in TILs and the upregulation of IFN-γ in tumor tissue are prognostic factors associated with a better clinical outcome following ICI treatment.[12,13,44] However, the present findings suggest that the loss of the secreting function for CXCL10/11 in tumor cells might inhibit the antitumor effects of ICIs, even in the high-TIL and IFN-γ rich tumors.

We also evaluated the usefulness of tumor-derived CXCL10/11 as a circulating predictive biomarker of ICI treatment. Inflammatory cytokines in peripheral blood have attracted attention as circulating biomarkers of immunotherapy for evaluating the tumor immune status both noninvasively and continuously. However, reports on the utility of cytokine biomarkers for assessing the outcome of ICI therapy have been limited, although cytokine gene expression profiles of tumor tissue, such as IFN-γ, CCL5, TGF-β, and CXCL9/10/11, have been shown to correlate with clinical response.[33,44-46] In NSCLC patients, the changes in serum levels of IL-6 and IL-8 by ICI treatment were shown to contribute to clinical outcomes,[18,19] but a pretreatment circulating biomarker that predicts the clinical outcome of ICI therapy is needed in order to facilitate personalized immunotherapy.

The present study has several potential clinical implications. First, based on our preclinical data generated using mouse models, the suppression of neovascularization and tumor hypoxia was observed only in tumors from ICI-responding mice. Therefore, the immunohistochemical evaluation of microvessel density might be useful for predicting the clinical outcome of patients treated with ICIs. Second, tumor-derived CXCL10/11 could be a key regulator of the sensitivity to anti-PD-1/PD-L1 therapy by not only recruiting effector CD8^{+} T cells but also by suppressing tumor angiogenesis. In addition, an in vitro study suggested that the CXCL10/11 production capacity of tumor cells in response to IFN-γ was required for the antitumor effects of PD-1/PD-L1 blockade in vivo. Thus, it could be instructive to focus on the sensitivity of tumor cells to IFN-γ in order to improve the efficacy of anti-PD-1/PD-L1 inhibitor. Third, the baseline serum CXCL10/11 levels could be useful as noninvasive biomarkers of sensitivity to anti-PD-1 Ab in NSCLC patients. However, there are several limitations in our study regarding this issue. First, the sample size used for the analysis of the correlation of serum CXCL10/11 level and the efficacy of ICIs in NSCLC patients is

too small to draw the conclusions. Second, recent therapy with ICIs against solid tumors including lung cancer has been shifted from ICI monotherapy to combined therapy with ICIs and other drugs, such as cytotoxic agents and molecular-targeted agents. Therefore, it is unclear whether the baseline serum CXCL10/11 levels are useful as predictive biomarkers of combined immunotherapy with ICIs.

In summary, we identified a novel mechanism for regulating the sensitivity to anti-PD-1/PD-L1 therapy, involving antiangiogenic effects through the production of tumor-derived CXCL10/11. Serum CXCL10/11 levels were also identified as noninvasive predictive biomarkers in both preclinical mouse models and NSCLC patients treated with anti-PD-1/PD-L1 inhibitors. These findings shed new light on the advent of personalized immunotherapy by monitoring the pretreatment immune status of individual patients.

DISCLOSURE

All authors declare no conflict of interest.

ORCID

Yasuhiko Nishioka https://orcid.org/0000-0001-6311-1654

REFERENCES

1. Ribas A, Wolchok JD. Cancer immunotherapy using checkpoint blockade. *Science*. 2018;359:1350-1355.
2. Hamid O, Robert C, Daud A, et al. Safety and tumor responses with lambrolizumab (anti-PD-1) in melanoma. *N Engl J Med*. 2013;369:134-144.
3. Carbone DP, Reck M, Paz-Ares L, et al. First-line nivolumab in stage IV or recurrent non-small-cell lung cancer. *N Engl J Med*. 2017;376:2415-2426.
4. Rittmeyer A, Barlesi F, Waterkamp D, et al. Atezolizumab versus docetaxel in patients with previously treated non-small-cell lung cancer (OAK): a phase 3, open-label, multicentre randomised controlled trial. *Lancet*. 2017;389:255-265.
5. Wei SC, Levine JH, Cogdill AP, et al. Distinct cellular mechanisms underlie anti-CTLA-4 and anti-PD-1 checkpoint blockade. *Cell*. 2017;170:1120-1133.
6. Huang AC, Postow MA, Orlowski RJ, et al. T-cell invigoration to tumour burden ratio associated with anti-PD-1 response. *Nature*. 2017;545:60-65.
7. Miller BC, Sen DR, Al Abosy R, et al. Subsets of exhausted CD8. *Nat Immunol*. 2019;20:326-336.
8. Yost KE, Satpathy AT, Wells DK, et al. Clonal replacement of tumor-specific T cells following PD-1 blockade. *Nat Med*. 2019;25:1251-1259.
9. Gordon SR, Maute RL, Dulken BW, et al. PD-1 expression by tumour-associated macrophages inhibits phagocytosis and tumour immunity. *Nature*. 2017;545:495-499.
10. Reck M, Rodríguez-Abreu D, Robinson AG, et al. Pembrolizumab versus chemotherapy for pd–l1–positive non-small-cell lung cancer. *N Engl J Med*. 2016;375:1823-1833.
11. Rizvi H, Sanchez-Vega F, La K, et al. Molecular determinants of response to anti-programmed cell death (PD)-1 and anti-programmed death-ligand 1 (PD-L1) blockade in patients with non-small-cell lung cancer profiled with targeted next-generation sequencing. *J Clin Oncol*. 2018;36:633-641.
12. Herbst RS, Soria J-C, Kowanetz M, et al. Predictive correlates of response to the anti-PD-L1 antibody MPDL3280A in cancer patients. *Nature*. 2014;515:563-567.
13. Havel JJ, Chowell D, Chan TA. The evolving landscape of biomarkers for checkpoint inhibitor immunotherapy. *Nat Rev Cancer*. 2019;19:133-150.
14. Finkelmeier F, Canli Ö, Tal A, et al. High levels of the soluble programmed death–ligand (sPD–L1) identify hepatocellular carcinoma patients with a poor prognosis. *Eur J Cancer*. 2016;59:152-159.
15. Okuma Y, Hosomi Y, Nakahara Y, Watanabe K, Sagawa Y, Homma S. High plasma levels of soluble programmed cell death ligand 1 are prognostic for reduced survival in advanced lung cancer. *Lung Cancer*. 2017;104:1-6.
16. Yamazaki N, Kiyohara Y, Uhara H, et al. Cytokine biomarkers to predict antitumor responses to nivolumab suggested in a phase 2 study for advanced melanoma. *Cancer Sci*. 2017;108:1022-1031.
17. Kamphorst AO, Pillai RN, Yang S, et al. Proliferation of PD-1 $^+$ CD8 T cells in peripheral blood after PD-1-targeted therapy in lung cancer patients. *Proc Natl Acad Sci USA*. 2017;114:4993-4998.
18. Sanmamed MF, Perez-Gracia JL, Schalper KA, et al. Changes in serum interleukin-8 (IL–8) levels reflect and predict response to anti-PD-1 treatment in melanoma and non-small cell lung cancer patients. *Ann Oncol*. 2017;28:1988-1995.
19. Ozawa Y, Amano Y, Kanata K, et al. Impact of early inflammatory cytokine elevation after commencement of PD-1 inhibitors to predict efficacy in patients with non-small cell lung cancer. *Med Oncol*. 2019;36:33.
20. Jin Y, Chauhan SK, El Annan J, et al. A novel function for programmed death ligand-1 regulation of angiogenesis. *Am J Pathol*. 2011;178:1922-1929.
21. Folkman J. Angiogenesis: an organizing principle for drug discovery? *Nat Rev Drug Discov*. 2007;6:273-286.
22. Carmeliet P, Jain RK. Molecular mechanisms and clinical applications of angiogenesis. *Nature*. 2011;473:298-307.
23. Georganaki M, van Hooren L, Dimberg A. Vascular targeting to increase the efficiency of immune checkpoint blockade in cancer. *Front Immunol*. 2018;9:3081.
24. Ciciola P, Cascetta P, Bianco C, Formisano L, Bianco R. Combining immune checkpoint inhibitors with anti-angiogenic agents. *J Clin Med*. 2020;9:675.
25. Susaki EA, Shimizu C, Kuno A, et al. Versatile whole-organ/body staining and imaging based on electrolyte-gel properties of biological tissues. *Nat Commun*. 2020;11:1982.
26. Weidner N, Semple JP, Welch WR, Folkman J. Tumor angiogenesis and metastasis–correlation in invasive breast carcinoma. *N Engl J Med*. 1991;324:1-8.
27. Vanzulli S, Gazzaniga S, Braidot MF, Vecchi A, Mantovani A, Wainstok de Calmanovici R. Detection of endothelial cells by MEC 13.3 monoclonal antibody in mice mammary tumors. *Biocell*. 1997;21:39-46.
28. Tokunaga R, Zhang WU, Naseem M, et al. CXCL9, CXCL10, CXCL11/CXCR3 axis for immune activation – a target for novel cancer therapy. *Cancer Treat Rev*. 2018;63:40-47.

29. Belperio JA, Keane MP, Arenberg DA, et al. CXC chemokines in angiogenesis. *J Leukoc Biol.* 2000;68:1-8.

30. Otsuka K, Mitsuhashi A, Goto H, et al. Anti-PD-1 antibody combined with chemotherapy suppresses the growth of mesothelioma by reducing myeloid-derived suppressor cells. *Lung Cancer.* 2020;146:86-96.

31. Chheda ZS, Sharma RK, Jala VR, Luster AD, Haribabu B. Chemoattractant receptors BLT1 and CXCR3 regulate antitumor immunity by facilitating CD8+ T cell migration into tumors. *J Immunol.* 2016;197:2016-2026.

32. Chow MT, Ozga AJ, Servis RL, et al. Intratumoral activity of the CXCR3 chemokine system is required for the efficacy of anti-PD-1 therapy. *Immunity.* 2019;50:1498-1512.

33. House IG, Savas P, Lai J, et al. Macrophage-derived CXCL9 and CXCL10 are required for antitumor immune responses following immune checkpoint blockade. *Clin Cancer Res.* 2020;26:487-504.

34. Palazon A, Tyrakis PA, Macias D, et al. An HIF-1α/VEGF-A axis in cytotoxic T cells regulates tumor progression. *Cancer Cell.* 2017;32:669-683.

35. Gropper Y, Feferman T, Shalit T, Salame TM, Porat Z, Shakhar G. Culturing CTLs under hypoxic conditions enhances their cytolysis and improves their anti-tumor function. *Cell Rep.* 2017;20:2547-2555.

36. de Almeida PE, Mak J, Hernandez G, et al. Anti-VEGF treatment enhances CD8+ T-cell antitumor activity by amplifying hypoxia. *Cancer Immunol Res.* 2020;8:806-818.

37. Zhang R, Tian L, Chen L-J, et al. Combination of MIG (CXCL9) chemokine gene therapy with low-dose cisplatin improves therapeutic efficacy against murine carcinoma. *Gene Ther.* 2006;13:1263-1271.

38. Feldman AL, Friedl J, Lans TE, et al. Retroviral gene transfer of interferon-inducible protein 10 inhibits growth of human melanoma xenografts. *Int J Cancer.* 2002;99:149-153.

39. Liu Z, Ravindranathan R, Li J, Kalinski P, Guo ZS, Bartlett DL. CXCL11-Armed oncolytic poxvirus elicits potent antitumor immunity and shows enhanced therapeutic efficacy. *Oncoimmunology.* 2016;5:e1091554.

40. Feldman ED, Weinreich DM, Carroll NM, et al. Interferon gamma-inducible protein 10 selectively inhibits proliferation and induces apoptosis in endothelial cells. *Ann Surg Oncol.* 2006;13:125-133.

41. Arenberg DA, White ES, Burdick MD, Strom SR, Strieter RM. Improved survival in tumor-bearing SCID mice treated with interferon-gamma-inducible protein 10 (IP-10/CXCL10). *Cancer Immunol Immunother.* 2001;50:533-538.

42. Manguso RT, Pope HW, Zimmer MD, et al. *In vivo* CRISPR screening identifies Ptpn2 as a cancer immunotherapy target. *Nature.* 2017;547:413-418.

43. Zaretsky JM, Garcia-Diaz A, Shin DS, et al. Mutations associated with acquired resistance to PD-1 blockade in melanoma. *N Engl J Med.* 2016;375(9):819-829.

44. Higgs BW, Morehouse CA, Streicher K, et al. Interferon gamma messenger RNA signature in tumor biopsies predicts outcomes in patients with non-small cell lung carcinoma or urothelial cancer treated with durvalumab. *Clin Cancer Res.* 2018;24:3857-3866.

45. Dangaj D, Bruand M, Grimm AJ, et al. Cooperation between constitutive and inducible chemokines enables T cell engraftment and immune attack in solid tumors. *Cancer Cell.* 2019;35:885-900.

46. Mariathasan S, Turley SJ, Nickles D, et al. TGFβ attenuates tumour response to PD-L1 blockade by contributing to exclusion of T cells. *Nature.* 2018;554:544-548.

SUPPORTING INFORMATION

Additional supporting information may be found in the online version of the article at the publisher's website.